Supplemental material to this article can be found at:
http://molpharm.aspetjournals.org/content/suppl/2021/09/09/molpharm.121.000357.DC1
1521-0111/100/5/480–490$35.00
MOLECULAR PHARMACOLOGY
https://doi.org/10.1124/molpharm.121.000357
Mol Pharmacol 100:480–490, November 2021

Construction and Characterization of CRISPR/Cas9 Knockout Rat Model of Carboxylesterase 2a Gene[S]

Jie Liu[1], Xuyang Shang[1], Shengbo Huang, Yuan Xu, Jian Lu, Yuanjin Zhang, Zongjun Liu, and Xin Wang

Shanghai Key Laboratory of Regulatory Biology, Institute of Biomedical Sciences and School of Life Sciences, East China Normal University, Shanghai, China (J.Li., X.S., S.H., Y.X., J.Lu., Y.Z., X.W.); and Department of Cardiology, Central Hospital of Shanghai Putuo District, Shanghai University of Traditional Chinese Medicine, Shanghai, China (Z.L.)

Received June 29, 2021; accepted August 30, 2021

ABSTRACT

Carboxylesterase (CES) 2, an important metabolic enzyme, plays a critical role in drug biotransformation and lipid metabolism. Although CES2 is very important, few animal models have been generated to study its properties and functions. Rat *Ces2* is similar to human *CES2A-CES3A-CES4A* gene cluster, with highly similar gene structure, function, and substrate. In this report, CRISPR-associated protein-9 (CRISPR/Cas9) technology was first used to knock out rat *Ces2a*, which is a main subtype of *Ces2* mostly distributed in the liver and intestine. This model showed the absence of CES2A protein expression in the liver. Further pharmacokinetic studies of diltiazem, a typical substrate of CES2A, confirmed the loss of function of CES2A both in vivo and in vitro. At the same time, the expression of CES2C and CES2J protein in the liver decreased significantly. The body and liver weight of *Ces2a* knockout rats also increased, but the food intake did not change. Moreover, the deficiency of *Ces2a* led to obesity, insulin resistance, and liver fat accumulation, which are consistent with the symptoms of nonalcoholic fatty liver disease (NAFLD). Therefore, this rat model is not only a powerful tool to study drug metabolism mediated by CES2 but also a good disease model to study NAFLD.

SIGNIFICANCE STATEMENT

Human carboxylesterase (CES) 2 plays a key role in the first-pass hydrolysis metabolism of most oral prodrugs as well as lipid metabolism. In this study, CRISPR/Cas9 technology was used to knock out *Ces2a* gene in rats for the first time. This model can be used not only in the study of drug metabolism and pharmacokinetics but also as a disease model of nonalcoholic fatty liver disease (NAFLD) and other metabolic disorders.

Introduction

Carboxylesterase (CES), a kind of α/β serine folding protein, is one of the most important phase I drug-metabolizing enzymes, belonging to the class B esterase (IMAI, 2006; Oda et al., 2015). The human CES superfamily is divided into five families (CES1, CES2, CES3, CES4A, CES5A), among which CES1 may exist in the form of monomer, trimer, or hexamer, whereas CES2 and CES3 mostly exist in the form of monomer (Kim et al., 1997; Fleming et al., 2007; Holmes et al., 2010). CES1 and CES2, as the main subtypes of carboxylesterase, have 47% amino acid sequence similarity. However, they have a clear tendency in the choice of substrates (Satoh and Hosokawa, 2006). CES1 tends to hydrolyze ester bonds with larger acyl moieties and smaller alcohol moieties, whereas CES2 prefers to select ester bond compounds with smaller acyl moieties and relatively large alcohol moieties as substrates (Di, 2019). CES2 is distributed widely in the small intestine, liver, colon, and kidney (Sato et al., 2012; Boberg et al., 2017). As one of the most abundant carboxylesterase subtypes in the gastrointestinal tract, CES2 mediates the first-pass hydrolysis metabolism of most oral prodrugs (Laizure et al., 2013), including a variety of clinical drugs, such as anticancer drugs capecitabine and flutamide (Xu et al., 2002; Abdelwahab et al., 2018), angiotensin receptor antagonists candesartan and olmesartan (Nishikawa et al., 1997; Ma et al., 2005), and many drugs affecting the central nerve system, such as heroin and cocaine

This work was supported in whole or part by grants from the National Natural Science Foundation of China [Grant 81773808], the Science and Technology Commission of Shanghai Municipality [Grant 18430760400], the China Postdoctoral Science Foundation [Grant 2020M671051], the Fundamental Research Funds for the Central Universities, and the Clinical Advantage Discipline of Health System of Putuo District in Shanghai. This work was also supported from East China Normal University (ECNU) Multifunctional Platform for Innovation [Grant 011] and the Instruments Sharing Platform of School of Life Sciences, East China Normal University.

[1]J. Li. and X.S. contributed equally to this work.

https://dx.doi.org/10.1124/molpharm.121.000357.

[S] This article has supplemental material available at molpharm.aspetjournals.org.

ABBREVIATIONS: ALP, alkaline phosphatase; ALT, alanine aminotransferase; AST, aspartate aminotransferase; AUC, area under the drug concentration-time curve; CES, carboxylesterase; CI, confidence interval; CRISPR/Cas9, CRISPR-associated protein-9 nuclease; DBL, direct bilirubin; GTT, glucose tolerance test; HDL-C, high-density lipoprotein cholesterol; IBIL, indirect bilirubin; ITT, insulin tolerance test; KO, knockout; LC-MS/MS, liquid chromatography with tandem mass spectrometry; LDL-C, low-density lipoprotein cholesterol; NAFLD, nonalcoholic fatty liver disease; PAM, protospacer adjacent motif; PCR, polymerase chain reaction; RLM, rat liver microsome; SD, Sprague-Dawley; sgRNA, single-guide RNA; TBA, total bile acid; TBL, total bilirubin; T-CH, total cholesterol; TG, triglyceride; WT, wild type.

(Kamendulis et al., 1996). Since the liver is the center of metabolism of most drugs in the body, especially drugs containing ester bonds, the total clearance of these drugs mainly depends on CES2. Inhibition of CES2 activity can lead to changes of drug exposure and result in serious side effects. With the emergence of clinical drugs containing ester bonds, more drug-drug interactions based on CES2 need to be further explored.

Human CES2 also plays an indispensable role in lipid metabolism. Lipid homeostasis regulated by CES2 is achieved through lipid hydrolysis, fatty acid oxidation, endoplasmic reticulum stress, and lipid synthesis (Lian et al., 2018). Previous studies have shown that the expression of CES2 in the liver of patients with nonalcoholic fatty liver disease (NAFLD) is significantly decreased, and the activity of CES2 is also decreased in patients who are obese (Li et al., 2016). However, transferring human CES2 into mice can significantly improve the disorder of liver lipid metabolism (Ruby et al., 2017). In addition, the expression of CES2 is directly or indirectly controlled by the activation of transcription factors, such as pregnane X receptor, constitutive active/androstane receptor, peroxisome proliferator-activated receptor -α, and hepatocyte nuclear factor 4α. These transcription factors are also closely related to the occurrence and development of NAFLD (Furihata et al., 2006; Staudinger et al., 2010), but the regulation of CES2 still needs further study. Therefore, it is an urgent need to establish reliable and practical animal models to study the role of CES2 in pathology and clinical medicine.

Rat *Ces2a* is the main subtype of *Ces2*, and its gene structure, function, and substrate are highly similar with humans. CRISPR-associated protein-9 nuclease (CRISPR/Cas9) technology, the third-generation artificial nuclease technology, has become a powerful gene-editing tool. Due to its practicability, simplicity, and high efficiency (Torres-Ruiz and Rodriguez-Perales, 2017), it is engineered for genome editing and then applied to the establishment of animal models, which greatly speeds up the pace of research (Hryhorowicz et al., 2017).

In this study, the *Ces2a* gene was knocked out in rats by CRISPR/Cas9 technology for the first time, and the *Ces2a* knockout (KO) rat model was successfully constructed and characterized. This model can be used not only in drug metabolism and pharmacokinetics but also as a disease model of metabolic disorder, such as NAFLD.

Materials and Methods

Reagents. Oligos (60 bp, containing *Ces2a* KO target sites) and all primers for polymerase chain reaction (PCR)/real-time PCR were synthesized by Biosune Biotechnology Co., Ltd (Shanghai, China). The SYBR Green real-time fluorescence quantitative PCR master mix and reverse transcription kit were purchased from Yeasen (Shanghai, China). T7 in vitro transcription kit and RNAiso Plus were bought from TaKaRa (Dalian, China). Bicinchoninic acid kit and SP6 in vitro transcription kit were obtained from Thermo Scientific (Waltham, MA). Blood glucose meter was from Johnson (New Brunswick, NJ). D-Glucose, insulin-human, and diltiazem were obtained from Meilun Biotech Co. Ltd (Dalian, China). Deacetyldiltiazem was bought from Toronto Research Chemicals Inc. (North York, ON, Canada).

Animals. Male and female Sprague-Dawley (SD) rats were purchased from National Rodent Laboratory Animal Resources (Shanghai, China). The animals were raised in a specific pathogen-free barrier with free access to rodent sterile water and chow cubes. The barrier was a humidity- and temperature-controlled environment with 12-hour light/dark cycles. All of the animal experiment protocols involved in this study were approved by the Ethics Committee on Animal Experimentation of East China Normal University (Shanghai, China).

Target-Site Selection. The sequence of *Ces2a* gene was obtained from the US National Center for Biotechnology Information (https://www.ncbi.nlm.nih.gov/pmc/). The gene ID (Ensembl, ENSRNOG00000011330) was submitted to the online website (https://benchling.com). The first exon sequence was selected for editing, and multiple 18-bp target sequences followed by a protospacer adjacent motif (PAM) site (5′-NGG-3′) in the 3′ end were obtained. Two sequences, 5′-TCTCCTCCAGCATGTGCA-3′ and 5′-TTGGCTAGACTTCCTGGT-3′ located upstream of the gene, were selected as the editing target gene.

In Vitro Synthesis of Single-Guide RNA and Cas9 mRNA. Firstly, a 60-bp oligo fragment including the T7 promotor and *Ces2a* target sequence was synthesized. Based on this fragment, the single-guide RNA (sgRNA) double-stranded template was constructed by overlapping PCR, and the products were then transcribed in vitro by the T7 transcription kit. Secondly, using the Cas9 plasmid as a template, Cas9 mRNA was constructed according to the instructions of SP6 in vitro transcription kit. Both the sgRNA of *Ces2a* and Cas9 mRNA were extracted and purified by phenol-chloroform methods and subsequently stored at −80°C for further application.

Comicroinjection of sgRNA and Cas9 mRNA into Zygote. Robust 8-week-old SD male rats were selected and caged with healthy 8-week-old SD female rats to collect fertilized eggs. The embryos were incubated in culture medium and 5% CO_2 for 2 hours at 37°C. Then, the mixture of *Ces2a* sgRNA (25 ng/μl) and Cas9 mRNA (50 ng/μl) was comicroinjected into the cytoplasm of the embryos. The injected embryos were cultured in the incubator for 2 hours, and the surviving embryos with intact cytoplasmic membrane and normal perivitelline space were transplanted into the oviducts of the pseudo-pregnant female rats.

Genotype Identification. The genomic DNA was extracted from the toes of newborn rats and then amplified by *Ces2a* primers (Table 1) with Easy-Taq DNA polymerase for identifying the genotypes of F0 chimeras with 1.5% agarose gel. PCR products with different bands were selected from wild-type (WT) rats for precise sequence and analyzed by DNAMAN (Lynnon Biosoft, San Ramon, CA). The F0 offspring carrying the expected mutations were caged with WT rats to obtain F1 generation. The genomic types of F1 rats were identified through direct sequencing of PCR products, and healthy adult F1 male and female rats with the same mutation were selected to mate to obtain F2 generation. The genomic types of F2 generation were identified by 1.5% agarose gel.

Off-Target Site Validation. The information of *Ces2a* target sites was submitted to the online website (https://benchling.com) to obtain potential off-target sites. Eight sites (Table 2) with relatively high off-targeting potential (score > 4.0) were selected for further analysis. Three homozygous KO rats and one WT rat were randomly selected for off-targeting analysis sequencing. The primers are listed in Table 1. The sequencing results were analyzed in DNAMAN.

mRNA Expression by PCR. Male *Ces2a* KO rats and WT rats (8 weeks old) were sacrificed by CO_2 asphyxiation. The liver and small intestine were collected and frozen at −80°C for further experimentation. Each unit of liver or small intestine (0.1 g) was homogenized by Automatic Sample Rapid Grinding Instrument (JXFSTPRP-24, Shanghai, China). The total mRNA was extracted according to the instruction of the Trizol method and then reverse-transcribed into cDNA. The obtained cDNA was used for PCR by *Ces2a* primers (Table 1) with Taq enzyme system, and the agarose gel electrophoresis was performed to validate the PCR results.

Protein Expression by Liquid Chromatography with Tandem Mass Spectrometry. Each unit of liver (0.1 g) was added with 400 μl lysate containing radioimmunoprecipitation assay, protease inhibitor, phosphatase inhibitor, and phenylmethanesulfonylfluoride,

TABLE 1
Primer pairs used in this research

No.	Primer Name	Primer Sequence (5′–3′)
1	*Ces2a*-F	CTGCTGGCTATTGGCTTCC
	Ces2a-R	CCTGCTGCTTTCCATCCC
2	*Ces2a*-OT-1-F	TCTCGATTACTTTTATAGACAC
	Ces2a-OT-1-R	CAGGGAAGGATACACCAT
3	*Ces2a*-OT-2-F	CTTTGAGATTATAGTGGGTT
	Ces2a-OT-2-R	AGATGGCCTACATCCTTA
4	*Ces2a*-OT-3-F	TTCCATCCCATAGGTTCA
	Ces2a-OT-3-R	GTGCCTTTGCTCTGACTG
5	*Ces2a*-OT-4-F	TTCAATAAGAACTTTGTCCCTC
	Ces2a-OT-4-R	CCCGGTTAATTTAAGCAGTA
6	*Ces2a*-OT-5-F	CTCAGAAGGACCAAGAAA
	Ces2a-OT-5-R	ATAGCCTAAGCTAAGGGA
7	*Ces2a*-OT-6-F	CTTGGTAGCTGGTGAGTC
	Ces2a-OT-6-R	TCCTATGGCTTCTGTCTT
8	*Ces2a*-OT-7-F	TTCCTCCTTCAGTTCCAC
	Ces2a-OT-7-R	GAGTTCCCACCTTCAAAA
9	*Ces2a*-OT-8-F	TTGGCAGAGCAGCATCAT
	Ces2a-OT-8-R	TGGCAGGAACCTCACAGA
10	*Ces1c*-F	ACTACAAACCTGGACAAGAAG
	Ces1c-R	GCAGTACCACTCCATCAATC
11	*Ces1d*-Q-F	CACTTCTGCTCTGATTACAAC
	Ces1d-Q-R	GGTTTCCAAGTAAATCCAG
12	*Ces1e*-Q-F	TCAATGACCTTCTAACTAACCG
	Ces1e-Q-R	TGGATGCCCCACCTAACACTAG
13	*Ces1f*-Q-F	CCTTCCTGGATTGTTAACC
	Ces1f-Q-R	TTATCCCTTTGTGAACTGAG
14	*Ces2a*-Q-F	CCTGCTTATTCTTATCCATGTG
	Ces2a-Q-R	GCCTACTTCATCCAGCATAT
15	*Ces2c*-Q-F	TAGCCCGACGAACTGAGA
	Ces2c-Q-R	GTCCTGACCCCACACATGG
16	*Ces2e*-Q-F	CTTTGCCAAGCCTCCTATAG
	Ces2e-Q-R	GTGGGCTGGTGTGTAGATGC
17	*Ces2h*-Q-F	GGATGTGAGCAGGTGGACTC
	Ces2h-Q-R	CTTCTTGGAGTCAGTGGTGG
18	*Ces2i*-Q-F	CTACAGACTGATATAATGAAGG
	Ces2i-Q-R	GTCCAGGTATCCCCAGTTGC
19	*Ces2j*-Q-F	GAATTGACCAAGCTTCCTATG
	Ces2j-Q-R	GTCCAGGTATCCCCAGTTGC
20	*Ces3a*-Q-F	CCTTATGGAAGTGCCCCCTG
	Ces3a-Q-R	AGGCTGACTTGAACTTCGCA
21	*β-actin*-Q-F	AGATCAAGATCATTGCTCCTCCT
	β-actin-Q-R	ACGCAGCTCAGTAACAGTCC

and then samples were homogenized and pyrolyzed at 4°C for 2 hours to extract total protein. After enzymatic hydrolysis at 37°C for 20 hours, samples were subsequently desalted and lyophilized, redissolved in 0.1% formic acid, and stored at −20°C for further use. Protein expression was detected by liquid chromatography with tandem mass spectrometry (LC-MS/MS) (Applied Protein Technology, Shanghai, China). The mass-to-charge ratios of peptides and peptide fragments were collected. A total of 20 fragments were collected after each full scan Atlas (MS2 scan) for database search. The mass of carboxylic ester hydrolase sequence (containing *Ces2a, Ces2c, Ces2j*) was 1582.7416. The mobile phase consisted of H_2O (A) and acetonitrile (B), both containing 0.1% formic acid (v/v), and 20 fragments were collected after each full scan. Data were processed and analyzed by Proteome Discoverer 1.4 (Thermo Fisher Scientific).

Detection of Compensatory Effects. Total RNA was extracted from the liver and small intestine of WT and KO rats by Trizol method according to the guidelines. Then, the concentration was measured with a NanoDrop 2000 spectrophotometer (Thermo Fisher Scientific). The total RNA was quantitatively reverse-transcribed into cDNA by using the Takara RR036A kit. The main subtypes of carboxylesterase were detected by real-time quantitative PCR using Quant Studio 3 Real-Time PCR System (Thermo Fisher Scientific). The primer information is listed in Table 1. The β-actin was set as the internal reference.

Body Weight. Male *Ces2a* $^{(-/-)}$ and WT rats were weighed once a week from the 3rd week to the 14th week. In addition, the liver weight at the age of 14 weeks was recorded.

Serum Biochemical Indexed Detection. To detect whether there were some physiologic changes in *Ces2a* KO rats, male *Ces2a* $^{(-/-)}$ and WT rats (8 and 14 weeks old, respectively) fasted for 12 hours before serum collection and drank sterile water freely. Blood samples were collected from the tail vein, and the serum biochemical indexes were detected by Shanghai ADICON Clinical Laboratories (Shanghai, China). Liver function indicators include total protein, albumin, globulin, albumin/globulin ratio, total bilirubin (TBL), direct bilirubin (DBL), indirect bilirubin (IBIL), aspartate aminotransferase (AST), alanine aminotransferase (ALT), AST/ALT, alkaline phosphatase (ALP), and total bile acid (TBA). Blood lipid indexes include triglyceride (TG), total cholesterol (T-CH), high-density lipoprotein cholesterol (HDL-C), and low-density lipoprotein cholesterol (LDL-C).

Glucose and Insulin Tolerance Tests. Glucose , a commonly used indicator of physiologic status, was also detected. In the glucose tolerance test (GTT), male *Ces2a* $^{(-/-)}$ and WT rats (14 weeks old) fasted for 16 hours with free access to sterile water. The glucose dissolved in sterilized saline was intraperitoneally injected into rats at a single dose of 2 g/kg. Blood samples were collected from tail vein both before injection and at 15, 30, 45, 60, 90, and 120 minutes after injection. The concentration of glucose was tested with blood glucose meter.

In the insulin tolerance test (ITT), male *Ces2a* $^{(-/-)}$ and WT rats (14 weeks old) fasted for 6 hours and drank sterile water freely. Insulin dissolved in acidic saline and then diluted by sterilized saline was intraperitoneally injected into rats at a single dose of 1 IU/ml. Blood samples were collected from tail vein both before injection and at 15, 30, 45, 60, and 90 minutes after injection. Blood glucose concentration was measured by a blood glucose meter.

Liver Staining. Male *Ces2a* $^{(-/-)}$ and WT rats (8 and 14 weeks old) were sacrificed. Liver tissue was carefully separated, cut into small pieces (1 cm × 1 cm × 0.5 cm), fixed with 4% paraformaldehyde PBS buffer, embedded in paraffin for cutting into 3-μm sections, and stained with H&E as well as Oil Red O according to the standard procedure.

Measurement of Lipids in Liver. Liver tissue (100 mg) from male *Ces2a* $^{(-/-)}$ rats at 14 weeks old was homogenized with 300 μl

TABLE 2
Details for all potential off-target sites

Name	Chromosome	Spacer	PAM	Off-Target Score
Ces2a sgRNA1	chr19	TTGGCTAGACTTCCTGGT	TGG	
Ces2a-OT-1	chr6	TGGACTAGACTTCCTGGT	GGG	5.5
Ces2a-OT-2	chr3	TTGTCTAGACTTCCTGCT	AAG	4.3
Ces2a sgRNA2	chr19	TCTCCTCCAGCATGTGCA	CGG	
Ces2a-OT-3	chr1	TCTGCTCCAGCATGTGCA	TGG	100
Ces2a-OT-4	chr19	TCTGCTCCAGCATGTGCA	TAG	100
Ces2a-OT-5	chr19	TCTCCTCCAGCATGTGCA	CGG	100
Ces2a-OT-6	chr19	TCTGCTCCAGCATGTGCA	TAG	100
Ces2a-OT-7	chr6	CCTCCTCAAGCATGTGCA	TAG	7.1
Ces2a-OT-8	chr1	CCTCCTGCAGCATGTGCA	TGG	4.6

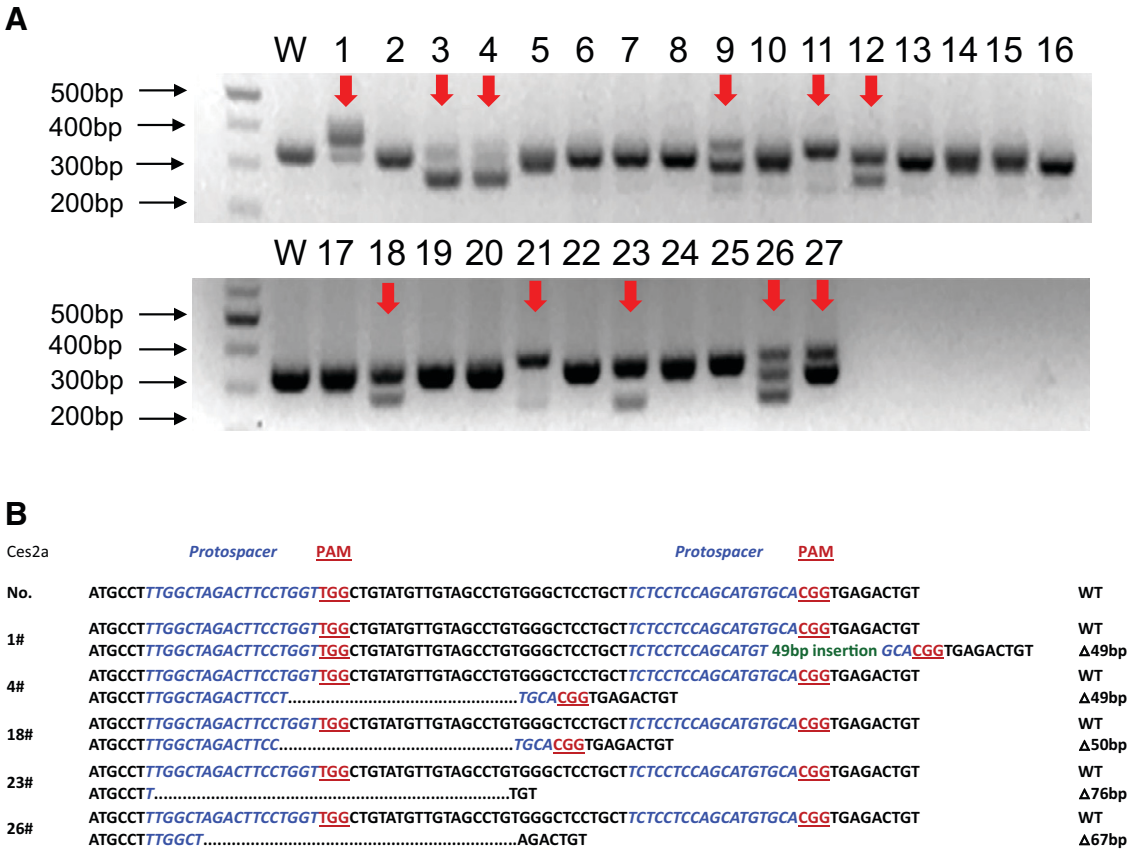

Fig. 1. Genotyping of the F0 generation of *Ces2a* KO rats generated by CRISPR/Cas9 system. (A) The mutations in the F0 generation for *Ces2a* were detected by 1.5% agarose gel using PCR products amplified from F0 rat toes genomic DNA by primer. "↓", mutation band; WT, negative control. (B) Analysis of *Ces2a* gene sequence of part of F0 generation rats. PCR products amplified from each F0 rat were sequenced. ".", nucleotide deletion; "△", the number of changed nucleotides; green words, nucleotide insertion.

methanol, and then lipids were extracted with 600 μl chloroform at 4°C for 12 hours. The mixture was centrifuged under 12,000 × g for 20 minutes at 4°C . The supernatant was subsequently transferred into a new centrifuge tube and dried under the atmosphere of nitrogen. The precipitation was reconstituted with alcohol to extract lipids and followed by detection by ADICON Clinical Laboratories.

In Vitro Determination of Ces2a Activity. The liver microsomes were prepared from 8-week-old male KO and WT rats, respectively. After comparing different protein concentrations and incubation time, we confirmed the optimal system. The incubation mixture included 0.5 mg/ml liver microsomes protein as well as 20–1000 μM diltiazem. The mixture was incubated in a 0.1 M phosphate buffer system, and the final volume was 300 μl. After preincubating at 37°C for 5 minutes, diltiazem was added to start the reaction. After incubation for 30 minutes, ice-cold acetonitrile (300 μl) containing 100 ng/ml verapamil (internal standard) was added to terminate the reaction. The mixture was centrifuged at 10,000 × g at 4°C for 15 minutes, and the supernatant was stored at −20°C for subsequent experiments.

In Vivo Determination of Ces2a Activity. The healthy 8-week-old male KO and WT rats were used in this study. The rats were given diltiazem at a single dose of 15 mg/kg (volume 5 ml/kg, dissolved in water) by gavage. Blood samples were collected from the tail vein at 0.08, 0.17, 0.5, 1, 2, 3, 4, 6, 8, 10, 12, and 24 hours after administration. The blood samples were centrifuged at 10,000 × g at 4°C for 15 minutes, and the supernatant was stored at −20°C for subsequent experiments.

Quantification of Diltiazem and Its Metabolite by LC-MS/MS. The LC-MS/MS system consisted of an Agilent 1290 HPLC-6470 triple quadrupole mass spectrometer coupled with an Agilent

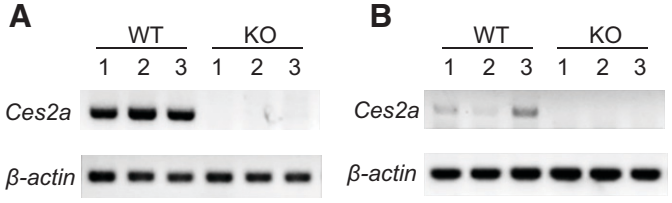

Fig. 2. Analysis of *Ces2a* expression in WT and KO rats (n = 3). (A) PCR analysis of *Ces2a* mRNA expression in livers of WT and KO rats. (B) PCR analysis of *Ces2a* mRNA expression in small intestines of WT and KO rats.

TABLE 3
Information on CES2A protein expression by LC-MS/MS

Name	Data
Mass (Da)	1582.7416
Gene names	*Ces2a; Ces2c; Ces2j*
Protein names	Carboxylic ester hydrolase
Intensity KO	0
Intensity WT	106,550,000
iBAQ KO	0
iBAQ WT	5.607.700
LFQ intensity KO	0
LFQ intensity WT	84,023,000

iBAQ, intensity-based absolute quantification; LFQ, label-free quantitation.

Jet Stream electrospray ionization ion source (Agilent Technologies, Santa Clara, CA). The chromatographic separation was performed on a Phenomenex Kinetex XB-C18 column (3 × 100 mm, 2.6 μm). The mobile phase consisted of H_2O (A) and acetonitrile (B), both containing 0.1% formic acid (v/v). Diltiazem metabolite and IS were eluted by high-performance liquid chromatography gradient: 0–3 minutes, 20%–70% B; 3–4 minutes, 70% B; 4–4.3 minutes, 70%–20% B. The flow rate was 0.3 ml/min and the injection volume was 2 μl. Diltiazem, deacetyldiltiazem, and IS were monitored in positive electrospray ionization mode, with the ion transitions of 415.1→165.1, 373.1→177.8, and 455.2→165.1, respectively .

Statistical Data Analysis. All data in this study were presented as mean ± S.D. The data were analyzed by two-tailed *t* test. GraphPad Prism 8.0 (GraphPad Software Inc., San Diego, CA) was used to plot mean plasma concentration-time curves. The pharmacokinetic parameters of diltiazem and its metabolite were calculated by WinNonlin 5.2.1 (Pharsight Corporation, Mountain View, CA) based on the noncompartmental model. The significant difference was considered when $P < 0.05$, expressed as $^*P < 0.05$, $^{**}P < 0.01$, and $^{***}P < 0.001$.

Results

Generation of Ces2a KO Rats. After the coinjection of *Ces2a* sgRNA and Cas9 mRNA, a total of 27 neonatal rats were obtained. We randomly numbered these 27 rats of the F0 generation from 1# to 27#. Then PCR and agarose gel electrophoresis were performed. As shown in Fig. 1A, multiple mutant alleles were identified among these founders, numbered as 1#, 3#, 4#, 9#, 11#, 12#, 18#, 21#, 23#, 26#, and 27#, indicating that a large fragment of the gene sequence had changed, which was then sequenced and analyzed. The peak patterns of 3#, 9#, 11#, 12#, 21#, and 27# were in a state of disorder and could not be analyzed. The remaining sequencing results are shown in Fig. 1B. The rats with nontriple base number changes in the exon region were selected for subsequent experiments. Since there was 69-bp deletion in 23# exon, F1 generation was obtained by crossing 1#, 4#, 18#, and 26# with WT rats. The genomic DNA of F1 generation was sequenced and analyzed. Healthy male and female rats with the same mutation were selected for mating to obtain F2 generation. After analysis of PCR products of F2 rats with 1.5% agarose gel, individuals with a homozygous deletion were obtained (Supplemental Fig. 1). In this study, KO rats after F2 generation were used for further study, and all WT rats were littermate rats of the KO rats.

Off-Target Analysis. Since CRISPR/Cas9 system allows 1–3 base pair mismatches in PAM-distal area, which may lead to off-target cleavage, the potential off-target sites were also detected. Three *Ces2a* KO rats were randomly selected to specifically amplify the potential off-target sites using eight pairs of designed primers (Table 1) and then sent to sequencing analysis. The results showed that *Ces2a* gene–edited rats were off-target at OT-5 (Supplemental Fig. 2). By

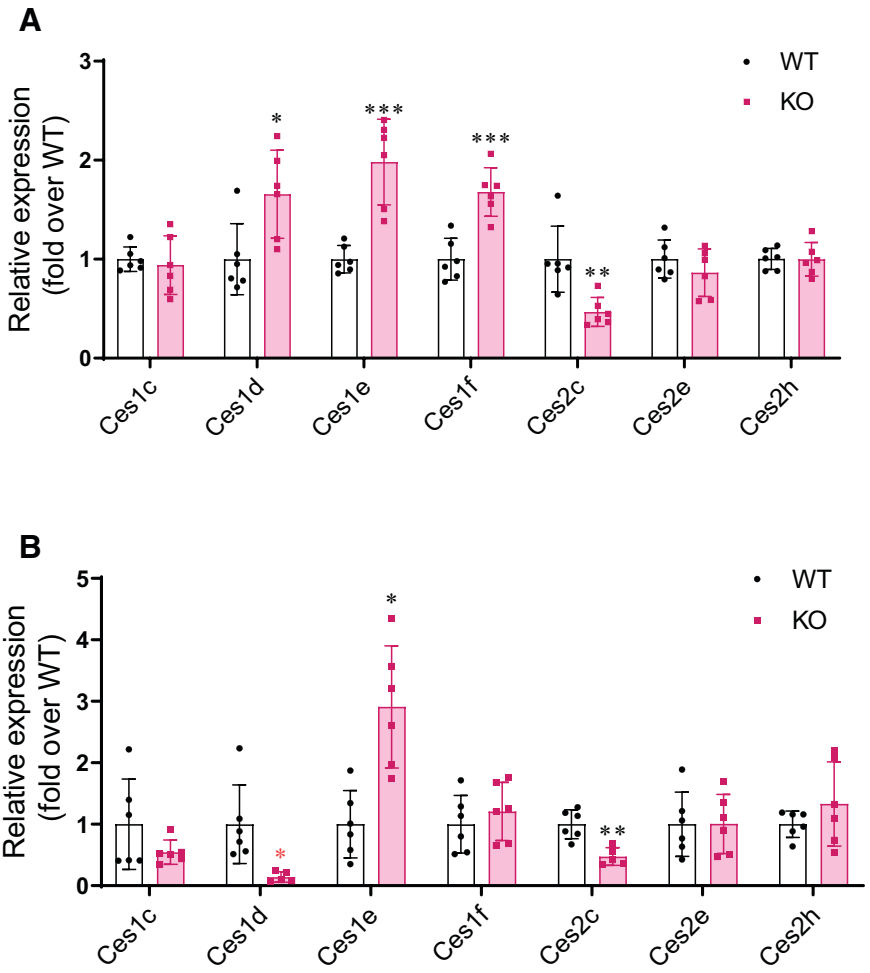

Fig. 3. Compensatory expression of other main *Ces* isoforms in *Ces2a* KO rats. (A) Compensatory expression in the liver. (B) Compensatory expression in the small intestine. All data were expressed as mean ± S.D. ($n = 6$). $^*P < 0.05$, $^{**}P < 0.01$, and $^{***}P < 0.001$ compared with WT group.

searching the US National Center for Biotechnology Information database, it was found that OT-5 did not belong to any gene. Therefore, there was no off-target in *Ces2a* KO rats.

Expression of Ces2a in WT and KO Rats. The expression of *Ces2a* in the liver of WT and KO rats was detected at mRNA and protein levels, respectively. The results showed that the *Ces2a* mRNA was completely absent in the liver (Fig. 2A) and small intestine (Fig. 2B) of KO rats. At the same time, the results of protein showed that compared with WT rats, KO rats did not express carboxylic ester hydrolase containing CES2A, CES2C, and CES2J (Table 3). These results confirmed that the construction of the *Ces2a* KO rat model was successful.

Compensatory Expression of Major Carboxylesterases in WT and KO Rats. To detect the compensatory expression of other major carboxylesterases after *Ces2a* gene knockout, we used real-time quantitative PCR to detect the mRNA levels of major carboxylesterases in rats. The results showed that in the liver, as compared with WT rats, the mean change in mRNA expression of *Ces1e*, *Ces1f*, and *Ces1d* increased by about 98% [95% confidence interval (CI) 53%–143%, $P < 0.001$], 67% (95% CI 43%–93%, $P < 0.001$), and 66% (95% CI 19%–110%, $P < 0.05$), respectively, and the expression of *Ces2c* decreased by about 53% (95% CI 38%–69%, $P < 0.01$) in KO rats (Fig. 3A). In the small intestine, the mRNA expression of *Ces1d* and *Ces2c* in KO rats also decreased by about 86% (95% CI 75%–97%, $P < 0.05$) and 52% (95% CI 35%–70%, $P < 0.01$), respectively (Fig. 3B).

Physiologic Conditions Detected in WT and KO Rats. Compared with WT rats, the body weight of *Ces2a* KO rats was higher from the 6th week (Fig. 4A), the liver weight was higher too at the 14th week (Fig. 4B), and the organ coefficient (liver weight/body weight) was also increased (Fig. 4C). At the same time, the livers of 8-week-old and 14-week-old KO and WT rats were stained with H&E. There was no statistically significant difference at the 8th week, but obvious lipid vacuoles as well as eosinophils appeared in the liver of KO rats at the 14th week (Fig. 4D), and the Oil Red O

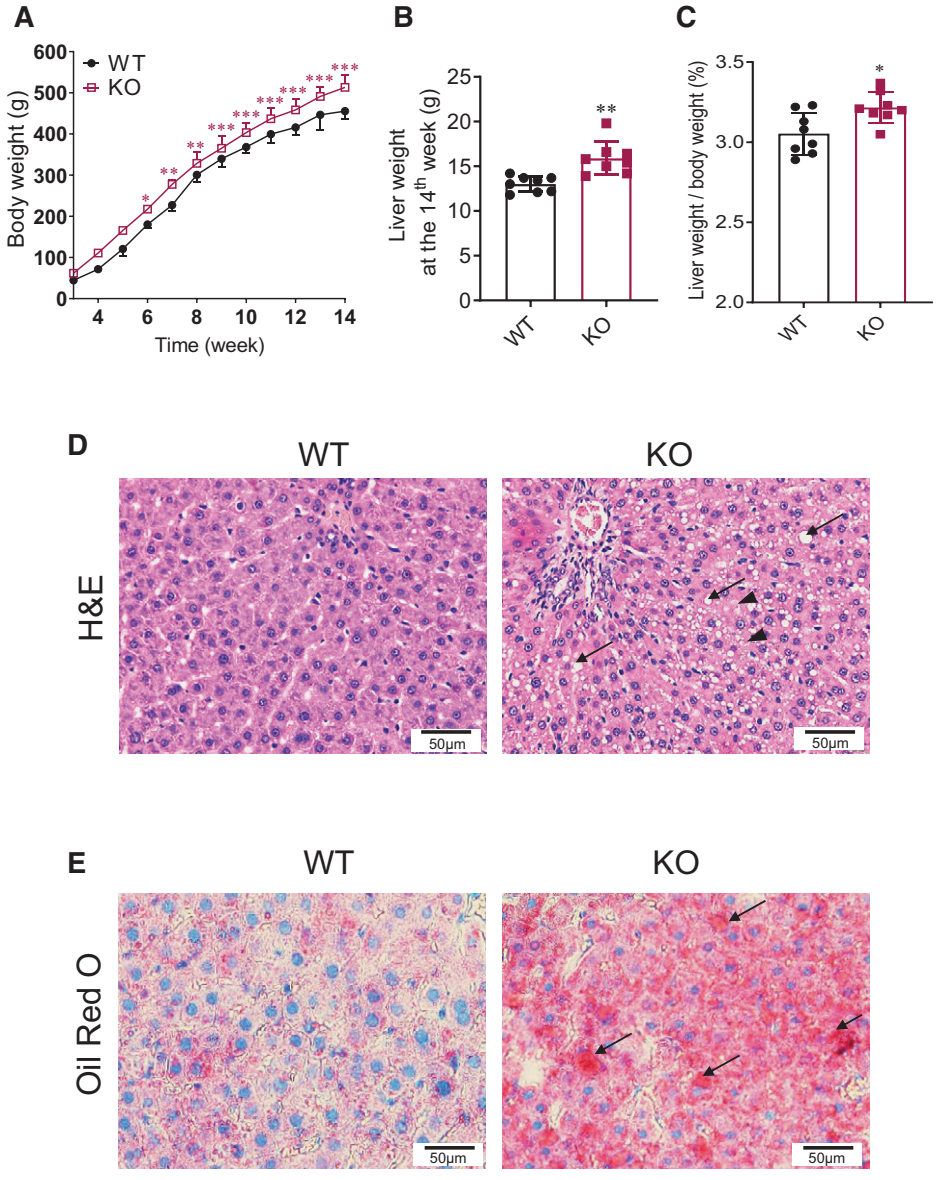

Fig. 4. (A) Body weight of WT and *Ces2a* KO rats from the 3rd week to the 14th week. Body weight was recorded once a week ($n = 8$). (B) Liver weight at the 14th week. Liver weight was determined and compared between WT and KO rats ($n = 8$) at 14 weeks of age. (C) Organ coefficient of liver. The liver organ coefficients of WT and KO rats were measured and compared. The ratio of liver weight/body weight was determined as the organ coefficient of liver. The results were shown as mean ± S.D. ($n = 8$). (D) Hematoxylin and eosin staining on liver sections from WT and KO rats at 14 weeks ($n = 6$). (E) Oil Red O staining on liver sections from WT and KO rats at 14 weeks ($n = 6$). "↓", lipid vacuoles; "■■■", eosinophils. *$P < 0.05$, **$P < 0.01$, and ***$P < 0.001$.

staining also showed more reddish liver in KO rats at the 14th week (Fig. 4E), indicating that there was more fat accumulation in the liver of KO rats.

Glucose and Insulin Tolerance Tests. The areas under the drug concentration-time curve (AUCs) of GTT and ITT of 14-week-old KO rats were 34% (95% CI 18%–50%, $P < 0.01$) and 53% (95% CI 38%–67%, $P < 0.001$) higher than those of WT rats, respectively (Fig. 5). These results showed that glucose and insulin sensitivity of *Ces2a* KO rats was lower than that of 14-week-old WT rats, indicating that the deletion of *Ces2a* deteriorated the glucose tolerance and insulin resistance.

Clinical Chemistry Analysis of WT and KO Rats. Due to the crucial role of *Ces2* in lipid metabolism, some important endogenous substances, such as bile acids and lipids, need to be detected. Moreover, if the *Ces2a* KO rats may be further used in the study of NAFLD, it is necessary to know whether the physiologic indexes of *Ces2a* KO rats have changed and whether the growth and reproduction of KO rats are normal. WT and KO rats (8 and 14 weeks old) were randomly selected for serum tests of liver function. At the 8th week, serum biochemistry data showed that TBL, DBL, IBIL, AST/ALT, ALP, TBA, TG, T-CH, HDL-C, and LDL-C levels of KO rats were all within 15% of the WT rats (Fig. 6A). At the 14th week, however, the levels of TBL, DBL, and IBIL in KO rats increased by 1.43-, 1.72-, and 1.63-fold, respectively (Fig. 6B). At the same time, the TBA increased significantly by 2.74-fold, and ALP increased by 1.25-fold. Moreover, the level of ALT in KO rats was higher than that of WT rats, and the level of AST/ALT was slightly lower than that of WT rats, indicating the occurrence of minor liver damage. There was no statistically significant difference in TG level. However, T-CH, HDL-C, and LDL-C all increased by nearly 1.50-fold, indicating the disorder of lipid metabolism, particularly cholesterol metabolism in KO rats (Fig. 6B). Except for the above indexes, liver protein synthesis levels of KO rats were all within 10% of WT (unpublished data). Lipids in livers of WT and KO rats at 14 weeks old were also detected. TG and LDL-C in livers of KO rats were 1.49- and 1.89-fold higher than that in WT rats, respectively, with no statistically significant difference in T-CH and HDL-C level, indicating heavy hepatic fat accumulation (Fig. 6C).

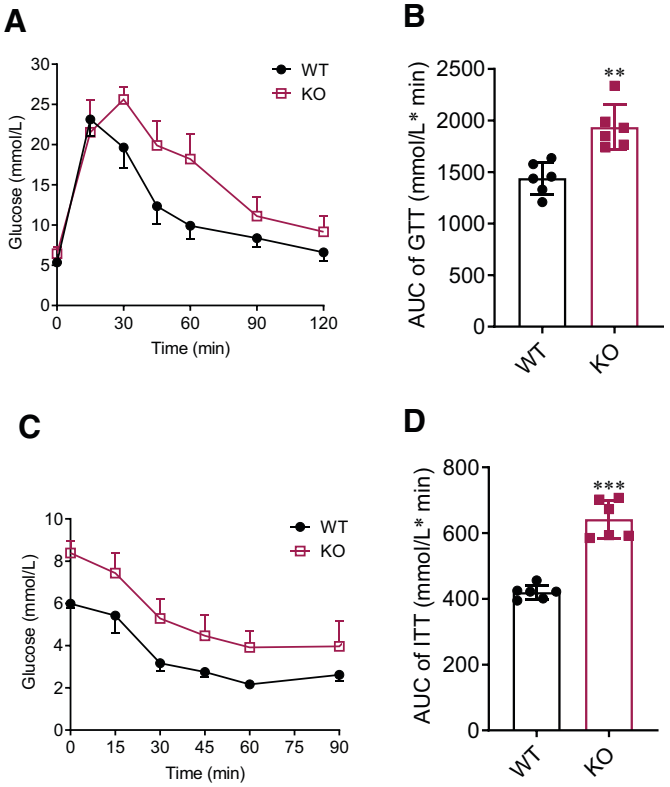

Fig. 5. Glucose and insulin tolerance of WT and *Ces2a* KO rats. (A and B) Glucose tolerance and AUC of GTT in WT and KO rats at 14 weeks of age. Serum samples were collected at 15, 30, 45, 60, 90, and 120 minutes after intraperitoneal injection of a dose of 2 g/kg glucose. (C and D) Insulin sensitivity and AUC of ITT in WT and KO rats at 14 weeks of age. Serum samples were collected at 15, 30, 45, 60, and 90 minutes after intraperitoneal injection of a single dose of 1 IU/ml insulin. The results were shown as mean ± S.D. of six rats. $^{**}P < 0.01$ and $^{***}P < 0.001$.

Determination of *Ces2a* Activity in WT and KO Rats. It is reported that diltiazem is metabolized by CES2A to produce its deacetylated metabolites in rats (Kurokawa et al., 2015). Using diltiazem as the substrate, the activity of CES2A in vitro and in vivo was determined by LC-MS/MS. In rat liver microsomes (RLMs) of both WT and KO rats, the capacity to metabolize diltiazem was detected (Fig. 7A). Compared with WT RLMs, V_{max} of diltiazem metabolism in KO RLMs (1.03 ± 0.47 nM/min/mg protein) was decreased by 87% compared with WT rats (7.78 ± 0.35 nM/min/mg protein) (Fig. 7B), and the intrinsic clearance of KO rats (0.54 ± 0.01 ml/min/kg) was also significantly reduced by 98% compared with WT rats (30.88 ± 0.51 ml/min/kg) (Fig. 7C). The results showed that compared with WT rats, the metabolic capacity of diltiazem in vitro in KO rats was significantly decreased.

To further assess the damaged function of CES2A in vivo in KO rats, pharmacokinetic experiments of diltiazem were carried out in WT and KO rats. After oral administration of diltiazem, there was no statistically significant difference between WT and KO rats (Fig. 7D). However, the pharmacokinetic parameters of deacetyldiltiazem showed crucial variation. Compared with WT rats, the C_{max} and $AUC_{0\text{-}24h}$ of KO rats were reduced by 98.7% and 97.3%, respectively (Table 4) (Fig. 7E). In addition, the mean residence time of KO rats increased by 78.0% compared with that in WT rats. The pharmacokinetic results of diltiazem in vivo were consistent with the data in vitro, which further confirmed the loss of function of CES2A in KO rats.

Discussion

In recent years, more and more attention has been paid to CES2, as it plays an important role in endogenous and exogenous metabolism (Frank et al., 1986; Di, 2019; Song et al., 2019; Yi et al., 2019). Because of the defects of in vitro and in vivo models, the study of CES2 is greatly limited. Cell models in vitro include primary cell and Caco-2 cell models (Di, 2019). The primary stem cell model has a complete metabolic enzyme system, which can simulate the physiologic environment of the body to a certain extent, but the cell culture conditions are strict and lack regulatory pathways (LeCluyse, 2001; Zhang et al., 2019). Additionally, the expression of CES2 in Caco-2 cell line is very different from that in humans, which cannot reflect the real situation of humans (Imai and Ohura, 2010; Ishizaki et al., 2018). In vivo models include inhibitor-inhibiting transporter activity and the gene editing model . However, the low specificity, high cost, and

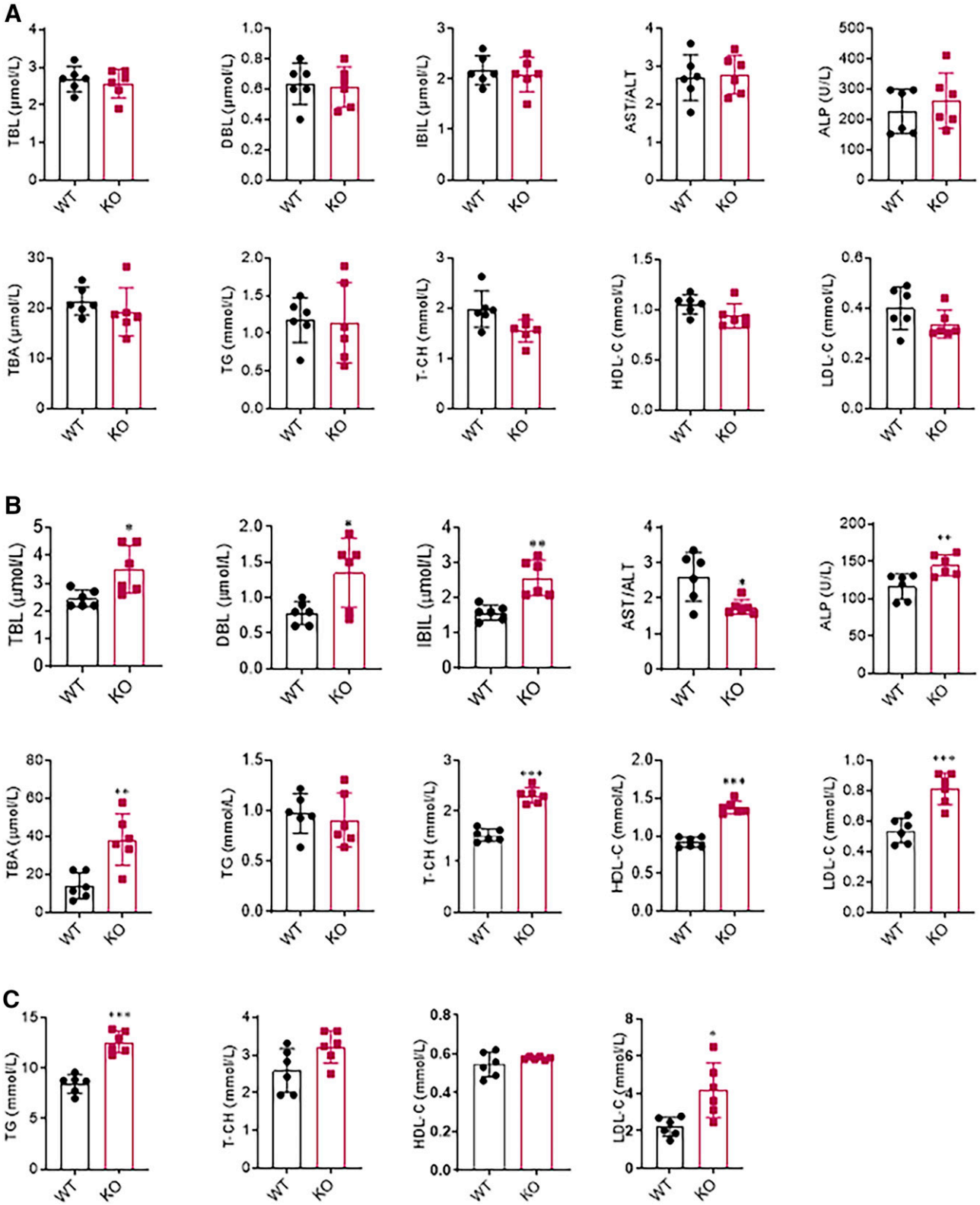

Fig. 6. Physiologic phenotype of *Ces2a* KO rats. (A) Clinical chemistry and physiologic analysis of serum from male WT and KO rats at 8 weeks old. (B) Clinical chemistry and physiologic analysis of serum from male WT and KO rats at 14 weeks old. (C) Hepatic lipids of WT and KO rats at 14 weeks old. HDL-C, LDL-C, TG, T-CH, TBA, AST, ALT, ALP, TBL, and DBL were compared between WT and KO rats. The results were shown as mean ± S.D. of six rats. $^{*}P < 0.05$, $^{**}P < 0.01$, and $^{***}P < 0.001$.

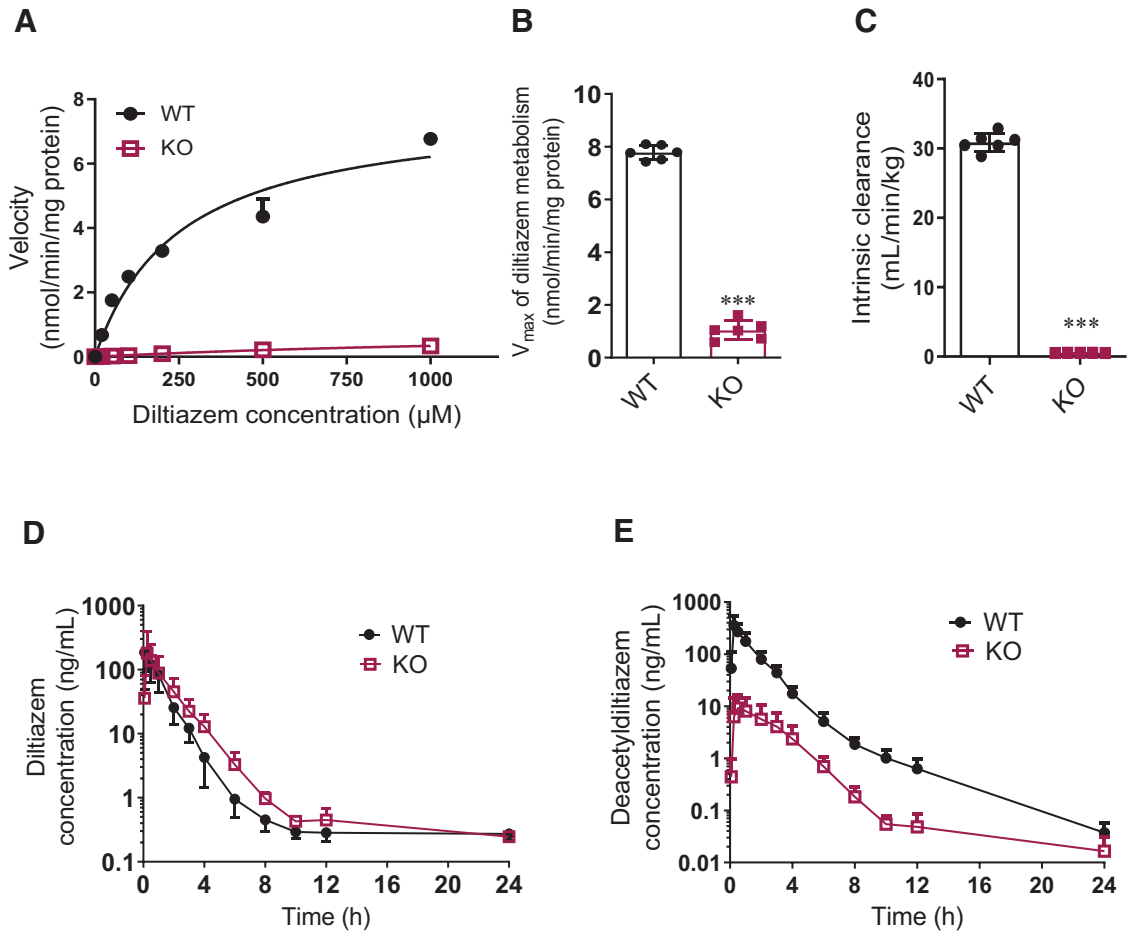

Fig. 7. CES2A-mediated catalytic activity of WT and KO rats in vitro and in vivo. (A) In vitro metabolism of diltiazem, a substrate of CES2A, by WT and KO RLMs. The *x*-axis represents the concentration of diltiazem. The *y*-axis represents the metabolic velocity of CES2A. (B) The V_{max} comparison of diltiazem metabolism in WT and KO RLMs. (C) The intrinsic clearance comparison of diltiazem metabolite in WT and KO RLMs. (D) The concentration vs. time profiles on pharmacokinetics of diltiazem in WT and KO rats. (E) The concentration vs. time profiles on pharmacokinetics of deacetyldiltiazem in WT and KO rats. All data were expressed as mean ± S.D. of six rats in each group. ***$P < 0.001$ compared with WT rats.

potential cytotoxicity of inhibitors make the results unreliable (Takahashi et al., 2009).

The gene editing model has attracted much attention because of its clearer genetic background and better reflecting the function of CES2. In 2019, intestine-specific *Ces2c* overexpression mice were generated for studying the function of intestinal *Ces2c* (Maresch et al., 2018). However, there is still no rat model of *Ces2* gene deletion. Compared with mice, rats have larger body size, stronger tolerance, and sufficient blood volume, and they are suitable for studying physiologic characteristics. In brief, the rat is a distinguished animal model for pharmacokinetic and toxicological studies (Wang et al., 2016; Ma et al., 2020). Compared with the early gene knockout technology based on homologous recombination, the CRISPR/Cas9 system has the advantages of high efficiency, simple operation, short circle, low cost, and high success rate, which greatly accelerate the development of gene editing (Cong et al., 2013; Wang et al., 2017; Lu et al., 2021). Therefore, CRISPR/Cas9 technology was the first choice for the construction of the *Ces2a* KO rat model in this study.

TABLE 4

Pharmacokinetic parameters of deacetyldiltiazem after oral administration of diltiazemThe dose of diltiazem was 15 mg/kg (p.o.). Results were mean ± S.D. of six rats.

Parameters	Unit	WT Rats	KO Rats
$t_{1/2}$	H	2.94 ± 0.72	2.45 ± 0.27
t_{max}	H	0.25	0.50
C_{max}	ng/ml	438.75 ± 138.04	5.69 ± 3.27***
$AUC_{0\text{-}24h}$	h*ng/ml	597.89 ± 91.89	15.66 ± 4.52***
$AUC_{0\text{-}inf}$	h*ng/ml	598.09 ± 92.01	15.74 ± 4.52***
$MRT_{0\text{-}24h}$	H	1.59 ± 0.12	2.83 ± 0.44**

MRT, mean residence time; t_{max}, peak time .
**$P < 0.01$ and ***$P < 0.001$ compared with WT rats.

Compared with WT rats, there was no expression of *Ces2a* mRNA in the liver of KO rats. Meanwhile, the expression of protein group (containing CES2A, CES2C, and CES2J) was also absent in the liver. In fact, at the mRNA expression level, *Ces2a*, *Ces2c*, and *Ces2e* are expressed in rat liver, whereas *Ces2j* is undetectable (Sanghani et al., 2002; Ohura et al., 2014). Moreover, the deletion of *Ces2a* caused the decreased mRNA expression of *Ces2c*, which may cause the reduced protein expression of CES2C in the KO rat. As a result, the deletion of *Ces2a*, no measurable level of *Ces2j*, and decreased protein expression of CES2C led to the

absence of protein group (containing CES2A, CES2C, and CES2J) in livers of KO rats. Combined with the absence of *Ces2a* in the livers and small intestines of KO rats in mRNA level, *Ces2a* KO rats were successfully generated. Our original goal was to knock out *Ces2a*, but we unexpectedly decreased the expression of *Ces2c* and *Ces2j*. Such a model may be more conducive to study the function of CES2. In addition, human blood lacks CES activity, whereas plasma derived from rodents is very proficient at CES substrate activation. Hence, animal models designed to predict tumor responses in humans may overestimate the efficacy of the drug because of the increased CES activity (Morton et al., 2005). Compared with the conditional knockout rat model, our *Ces2a* KO rats may represent a more accurate model for drug metabolism.

Since CES2 was age-dependent (Hines et al., 2016), liver H&E staining and serum physiologic indexes of liver function were detected in 8- and 14-week-old rats. There was no significant difference of the baseline body weights between WT and KO rats; however, during the course of this study, KO rats showed continuous weight gain and were finally significantly heavier than WT rats, showing the characteristic of obesity. Meanwhile, the H&E and Oil Red O staining of rats at 14 weeks old showed heavy fat accumulation, minor eosinophils, and enlargement of hepatic sinusoids in KO rats, which confirmed the hepatic fat accumulation. To further explore the influence of *Ces2a* on the liver, subsequent tests were conducted on 14-week-old rats, and the results showed that glucose and insulin sensitivity of *Ces2a* KO rats were significantly lower than those of 14-week-old WT rats, indicating the loss of *Ces2a* deteriorated the glucose tolerance and insulin resistance. At the same time, the results of physiologic indexes showed that AST/ALT decreased in KO rats, suggesting the liver damage occurred in KO rats at 14 weeks old. In addition, T-CH, LDL-C, TBA, and ALP in 14-week-old KO rats were significantly higher than those in WT rats, indicating that the loss of *Ces2a* led to the disorder of cholesterol metabolism, which may also be the cause of hepatic fat accumulation and liver injury. Surprisingly, the level of HDL-C was also significantly upregulated. To maintain the balance of cholesterol, the body needs to produce more HDL-C and bring the excess cholesterol deposited in the peripheral tissue back to the liver to regulate redistribution of cholesterol. Hepatic lipids detection showed significantly increased TG and LDL-C level in KO rats at 14 weeks old, which was consistent with the serum detection. These results suggested that KO rats showed the features of obesity, hyperglycemia/insulin resistance, and hepatic fat accumulation, which were also characteristics of an ideal NAFLD model (Jahn et al., 2019). The close relationship between *Ces2a* and lipid metabolism may lead to the occurrence of NAFLD. Moreover, with the increase of age, *Ces2a* is more involved in the metabolism of endogenous substances. However, the regulatory effect of *Ces2a* on lipid metabolism remains to be further studied.

We further used diltiazem, a selective substrate of CES2A, to verify the change of its function in KO rats. In humans, diltiazem is primarily metabolized to *N*-demethyldiltiaze, *O*-demethyldiltiazem, and deacetyldiltiazem through CYP3A4, CYP2D6, and esterase. The AUC ration of the metabolites is 1:3.4:28, respectively (Molden et al., 2002). Although esterase plays an important role in the deacetylation of diltiazem, it has not been identified so far. Previous studies have reported that four carboxylesterase enzymes (CES1D, CES1E, CES1F, and CES2A) in rats are identified as potential candidate deacetylases of diltiazem, but the CES2A enzyme is considered to be the main enzyme responsible for diltiazem deacetylation (Kurokawa et al., 2015). Therefore, although the compensatory effects were observed in KO rats, the deacetylase of diltiazem by CES2A in RLMs was not affected. Both in vitro and in vivo experiments demonstrated the loss of function of CES2A in KO rats.

At present, different animal models have been constructed to simulate NAFLD, such as the genetic model, the nutrient-deficient model, and models based on obesogenic high-fat diets. However, these models are limited by the disadvantages of overly artificial diets, vague genetic background, or unclear epidemiology (Jahn et al., 2019). Since there is no approved drug for NAFLD, there is an urgent need to identify promising pharmacological targets and develop future therapies. Our *Ces2a* KO rats have the characteristics of obesity, hyperglycemia, insulin resistance, and hepatic fat accumulation, which may be an ideal NAFLD model. It has the advantages of clear genetic background, clear epidemiology, short feeding period, and no additional artificial diets.

In conclusion, the *Ces2a* KO rat model was successfully established by CRISPR/Cas9 technology for the first time. This model can be used in the study of drug metabolism and pharmacokinetics. At the same time, it has the characteristics related to NAFLD and is a good disease model for the study of NAFLD. Using this animal model, we can better understand the role of CES2 in drug metabolism and lipid metabolism.

Authorship Contributions

Participated in research design: Wang.
Conducted experiments: J. Liu, Shang, Huang, Xu.
Performed data analysis: J. Liu, Shang, Z. Liu, Wang.
Wrote or contributed to the writing of the manuscript: J. Liu, Lu, Zhang, Wang.

References

Abdelwahab NS, Elshemy HAH, and Farid NF (2018) Determination of flutamide and two major metabolites using HPLC-DAD and HPTLC methods. *Chem Cent J* **12**:4.

Boberg M, Vrana M, Mehrotra A, Pearce RE, Gaedigk A, Bhatt DK, Leeder JS, and Prasad B (2017) Age-dependent absolute abundance of hepatic carboxylesterases (CES1 and CES2) by LC-MS/MS proteomics: application to PBPK modeling of oseltamivir in vivo pharmacokinetics in infants. *Drug Metab Dispos* **45**:216–223.

Cong L, Ran FA, Cox D, Lin S, Barretto R, Habib N, Hsu PD, Wu X, Jiang W, Marraffini LA, et al. (2013) Multiplex genome engineering using CRISPR/Cas systems. *Science* **339**:819–823.

Di L (2019) The impact of carboxylesterases in drug metabolism and pharmacokinetics. *Curr Drug Metab* **20**:91–102.

Fleming CD, Edwards CC, Kirby SD, Maxwell DM, Potter PM, Cerasoli DM, and Redinbo MR (2007) Crystal structures of human carboxylesterase 1 in covalent complexes with the chemical warfare agents soman and tabun. *Biochemistry* **46**:5063–5071.

Frank N, Caesar R, Scherf HR, and Wiessler M (1986) Influence of the carboxylesterase inhibitor bis-p-nitrophenylphosphate on the rates of hydrolysis of various alpha-esters of 1-(N-methyl-N-nitrosamino)-methanol in vitro and in vivo and on the acute toxicity and carcinogenicity of 1-(N-methyl-N-nitrosamino)-methylacetate. *J Cancer Res Clin Oncol* **111**:98–102.

Furihata T, Hosokawa M, Masuda M, Satoh T, and Chiba K (2006) Hepatocyte nuclear factor-4alpha plays pivotal roles in the regulation of mouse carboxylesterase 2 gene transcription in mouse liver. *Arch Biochem Biophys* **447**:107–117.

Hines RN, Simpson PM, and McCarver DG (2016) Age-dependent human hepatic carboxylesterase 1 (CES1) and carboxylesterase 2 (CES2) postnatal ontogeny. *Drug Metab Dispos* **44**:959–966.

Holmes RS, Wright MW, Laulederkind SJ, Cox LA, Hosokawa M, Imai T, Ishibashi S, Lehner R, Miyazaki M, Perkins EJ, et al. (2010) Recommended nomenclature for five mammalian carboxylesterase gene families: human, mouse, and rat genes and proteins. *Mamm Genome* **21**:427–441.

Hryhorowicz M, Lipiński D, Zeyland J, and Słomski R (2017) CRISPR/Cas9 immune system as a tool for genome engineering. *Arch Immunol Ther Exp (Warsz)* **65**:233–240.

Imai T (2006) Human carboxylesterase isozymes: catalytic properties and rational drug design. *Drug Metab Pharmacokinet* **21**:173–185.
Imai T and Ohura K (2010) The role of intestinal carboxylesterase in the oral absorption of prodrugs. *Curr Drug Metab* **11**:793–805.
Ishizaki Y, Furihata T, Oyama Y, Ohura K, Imai T, Hosokawa M, Akita H, and Chiba K (2018) Development of a Caco-2 cell line carrying the human intestine-type CES expression profile as a promising tool for ester-containing drug permeability studies. *Biol Pharm Bull* **41**:697–706.
Jahn D, Kircher S, Hermanns HM, and Geier A (2019) Animal models of NAFLD from a hepatologist's point of view. *Biochim Biophys Acta Mol Basis Dis* **1865**:943–953.
Kamendulis LM, Brzezinski MR, Pindel EV, Bosron WF, and Dean RA (1996) Metabolism of cocaine and heroin is catalyzed by the same human liver carboxylesterases. *J Pharmacol Exp Ther* **279**:713–717.
Kim KK, Song HK, Shin DH, Hwang KY, Choe S, Yoo OJ, and Suh SW (1997) Crystal structure of carboxylesterase from Pseudomonas fluorescens, an alpha/beta hydrolase with broad substrate specificity. *Structure* **5**:1571–1584.
Kurokawa T, Fukami T, and Nakajima M (2015) Characterization of species differences in tissue diltiazem deacetylation identifies Ces2a as a rat-specific diltiazem deacetylase. *Drug Metab Dispos* **43**:1218–1225.
Laizure SC, Herring V, Hu Z, Witbrodt K, and Parker RB (2013) The role of human carboxylesterases in drug metabolism: have we overlooked their importance? *Pharmacotherapy* **33**:210–222.
LeCluyse EL (2001) Human hepatocyte culture systems for the in vitro evaluation of cytochrome P450 expression and regulation. *Eur J Pharm Sci* **13**:343–368.
Li Y, Zalzala M, Jadhav K, Xu Y, Kasumov T, Yin L, and Zhang Y (2016) Carboxylesterase 2 prevents liver steatosis by modulating lipolysis, endoplasmic reticulum stress, and lipogenesis and is regulated by hepatocyte nuclear factor 4 alpha in mice. *Hepatology* **63**:1860–1874.
Lian J, Nelson R, and Lehner R (2018) Carboxylesterases in lipid metabolism: from mouse to human. *Protein Cell* **9**:178–195.
Lu J, Liu J, Guo Y, Zhang Y, Xu Y, and Wang X (2021) CRISPR-Cas9: a method for establishing rat models of drug metabolism and pharmacokinetics. *Acta Pharm Sin B*, in press.
Ma SF, Anraku M, Iwao Y, Yamasaki K, Kragh-Hansen U, Yamaotsu N, Hirono S, Ikeda T, and Otagiri M (2005) Hydrolysis of angiotensin II receptor blocker prodrug olmesartan medoxomil by human serum albumin and identification of its catalytic active sites. *Drug Metab Dispos* **33**:1911–1919.
Ma X, Shang X, Qin X, Lu J, Liu M, and Wang X (2020) Characterization of organic anion transporting polypeptide 1b2 knockout rats generated by CRISPR/Cas9: a novel model for drug transport and hyperbilirubinemia disease. *Acta Pharm Sin B* **10**:850–860.
Maresch LK, Benedikt P, Feiler U, Eder S, Zierler KA, Taschler U, Kolleritsch S, Eichmann TO, Schoiswohl G, Leopold C, et al. (2018) Intestine-specific overexpression of carboxylesterase 2c protects mice from diet-induced liver steatosis and obesity. *Hepatol Commun* **3**:227–245.
Molden E, Johansen PW, Bøe GH, Bergan S, Christensen H, Rugstad HE, Rootwelt H, Reubsaet L, and Lehne G (2002) Pharmacokinetics of diltiazem and its metabolites in relation to CYP2D6 genotype. *Clin Pharmacol Ther* **72**:333–342.
Morton CL, Iacono L, Hyatt JL, Taylor KR, Cheshire PJ, Houghton PJ, Danks MK, Stewart CF, and Potter PM (2005) Activation and antitumor activity of CPT-11 in plasma esterase-deficient mice. *Cancer Chemother Pharmacol* **56**:629–636.
Nishikawa K, Naka T, Chatani F, and Yoshimura Y (1997) Candesartan cilexetil: a review of its preclinical pharmacology. *J Hum Hypertens* **11** (Suppl 2):S9–S17.
Oda S, Fukami T, Yokoi T, and Nakajima M (2015) A comprehensive review of UDP-glucuronosyltransferase and esterases for drug development. *Drug Metab Pharmacokinet* **30**:30–51.
Ohura K, Tasaka K, Hashimoto M, and Imai T (2014) Distinct patterns of aging effects on the expression and activity of carboxylesterases in rat liver and intestine. *Drug Metab Dispos* **42**:264–273.
Ruby MA, Massart J, Hunerdosse DM, Schönke M, Correia JC, Louie SM, Ruas JL, Näslund E, Nomura DK, and Zierath JR (2017) Human carboxylesterase 2 reverses obesity-induced diacylglycerol accumulation and glucose intolerance. *Cell Rep* **18**:636–646.
Sanghani SP, Davis WI, Dumaual NG, Mahrenholz A, and Bosron WF (2002) Identification of microsomal rat liver carboxylesterases and their activity with retinyl palmitate. *Eur J Biochem* **269**:4387–4398.
Sato Y, Miyashita A, Iwatsubo T, and Usui T (2012) Simultaneous absolute protein quantification of carboxylesterases 1 and 2 in human liver tissue fractions using liquid chromatography-tandem mass spectrometry. *Drug Metab Dispos* **40**:1389–1396.
Satoh T and Hosokawa M (2006) Structure, function and regulation of carboxylesterases. *Chem Biol Interact* **162**:195–211.
Song YQ, Guan XQ, Weng ZM, Wang YQ, Chen J, Jin Q, Fang SQ, Fan B, Cao YF, Hou J, et al. (2019) Discovery of a highly specific and efficacious inhibitor of human carboxylesterase 2 by large-scale screening. *Int J Biol Macromol* **137**:261–269.
Staudinger JL, Xu C, Cui YJ, and Klaassen CD (2010) Nuclear receptor-mediated regulation of carboxylesterase expression and activity. *Expert Opin Drug Metab Toxicol* **6**:261–271.
Takahashi S, Katoh M, Saitoh T, Nakajima M, and Yokoi T (2009) Different inhibitory effects in rat and human carboxylesterases. *Drug Metab Dispos* **37**:956–961.
Torres-Ruiz R and Rodriguez-Perales S (2017) CRISPR-Cas9 technology: applications and human disease modelling. *Brief Funct Genomics* **16**:4–12.
Wang HX, Li M, Lee CM, Chakraborty S, Kim HW, Bao G, and Leong KW (2017) CRISPR/Cas9-based genome editing for disease modeling and therapy: challenges and opportunities for nonviral delivery. *Chem Rev* **117**:9874–9906.
Wang X, Tang Y, Lu J, Shao Y, Qin X, Li Y, Wang L, Li D, and Liu M (2016) Characterization of novel cytochrome P450 2E1 knockout rat model generated by CRISPR/Cas9. *Biochem Pharmacol* **105**:80–90.
Xu G, Zhang W, Ma MK, and McLeod HL (2002) Human carboxylesterase 2 is commonly expressed in tumor tissue and is correlated with activation of irinotecan. *Clin Cancer Res* **8**:2605–2611.
Yi J, Bai R, An Y, Liu TT, Liang JH, Tian XG, Huo XK, Feng L, Ning J, Sun CP, et al. (2019) A natural inhibitor from Alisma orientale against human carboxylesterase 2: kinetics, circular dichroism spectroscopic analysis, and docking simulation. *Int J Biol Macromol* **133**:184–189.
Zhang L, Liang C, Xu P, Liu M, Xu F, and Wang X (2019) Characterization of in vitro Mrp2 transporter model based on intestinal organoids. *Regul Toxicol Pharmacol* **108**:104449.

Address correspondence to: Dr. Xin Wang, Dongchuan Rd. 500, Shanghai, 200241, China. Email: xwang@bio.ecnu.edu.cn; or Dr. Zongjun Liu. Email: lzj72@126.com

Construction and characterization of CRISPR/Cas9 knockout rat model of carboxylesterase 2a gene

Jie Liu[a,#], Xuyang Shang[a,#], Shengbo Huang[a], Yuan Xu[a], Jian Lu[a], Yuanjin Zhang[a], Zongjun Liu[b,*], Xin Wang[a,*]

[a]Shanghai Key Laboratory of Regulatory Biology, Institute of Biomedical Sciences and School of Life Sciences, East China Normal University, Shanghai 200241, China

[b]Department of Cardiology, Central Hospital of Shanghai Putuo District, Shanghai University of Traditional Chinese Medicine, Shanghai 200062, China.

[#]These authors contributed equally to this work.

Supplementary Figures

Fig. S1. Gene sequence near the target in WT and *Ces2a* KO rats.

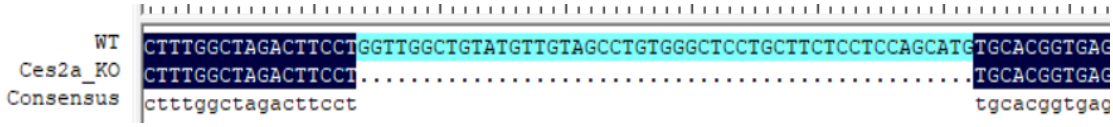

".", missing sequence.

Fig. S2. Off-target analysis of CRISPR/Cas9 induced mutation in three *Ces2a* knockout rats.

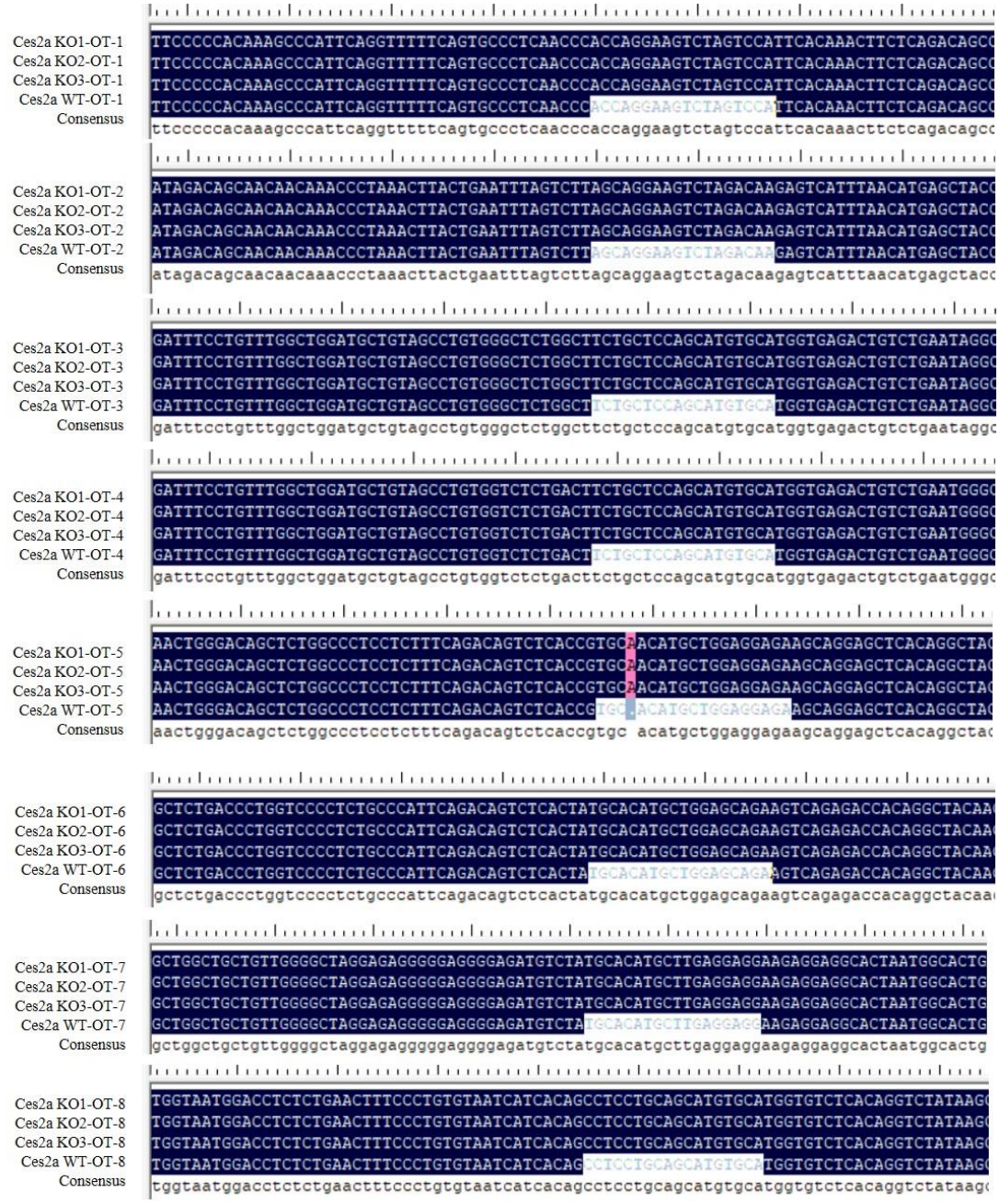

Eight OTS for *Ces2a* sgRNA were selected for sequence analysis. After searching the NCBI, it was found that OT-5 did not belong to any gene, so there was no off-target in *Ces2a* KO rats. Red box, sequence analysis of off-target sites; ".", missing sequence.